LA-UR-12-26566
Approved for public release; distribution is unlimited.

Title: A Consistent Approach to Modeling MHD-driven Cylindrical Damage Experiments

Author(s): Kaul, Ann

Intended for: Megagauss 2012, 2012-10-14/2012-10-19 (Maui, Hawaii, United States)

A Consistent Approach to Modeling MHD-driven Cylindrical Damage Experiments

Ann M. Kaul
Los Alamos National Laboratory, P.O. Box 1663 – MS 663
Los Alamos, NM 87545 USA

Abstract:
Well-characterized experimental data is essential for development of models describing complex material processes such as damage and failure. There is currently a dearth of experimental data capturing material behavior for the processes of non-uniaxial loading to failure and void closure after damage. LANL and VNIIEF recently completed a series of ten helical-generator-driven cylindrical damage experiments using high-precision diagnostics to measure the drive conditions and the material response. These experiments produced a well-characterized damage data set ranging from void initiation to complete failure and recollection for a well-studied material, aluminum. Combining magneto-hydrodynamics (MHD) and material modeling capabilities in a Lagrangian hydrocode allows for self-consistent end-to-end simulations of MHD-driven material property experiments. Simulation results for the damage experiments compared to experimental data will be presented.

I. Introduction

Development of models describing complex material processes such as damage and failure in ductile materials requires well-characterized experimental data. Experiments provide the data necessary both to produce model parameter values for specific materials and to validate encoded computational models. There is limited experimental failure data available in two regimes: (1) the mechanisms which control the onset of void formation and growth for multidimensional configurations and (2) the properties of a damaged material where reacceleration of the native material leads to void closure after damage. A series of ten cylindrical damage experiments was recently completed with aluminum.

Simulations of such experiments require codes which contain all of the relevant physics. LANL has recently implemented resistive diffusion and ohmic heating capabilities into its hydrodynamic simulation codes. LANL has fielded numerous MHD experiments studying material properties such as strength, damage and friction. Combining MHD capabilities with material modeling capabilities in a hydrocode allows for self-consistent end-to-end simulations of MHD-driven material property experiments. Following a brief description of the experiments and code models, simulation results of the damage experiments will be compared to experimental data.

II. Cylindrical Damage Experiments

A magnetically-driven cylindrical configuration has several advantages over traditional planar experiments, usually loaded by gas gun flyers or high explosive products. A convergent geometry, such as a cylinder, obviously allows access to multi-dimensional stress states. Simultaneously, cylindrical geometry offers natural recollection of the damaged material as the motion of the spallation layer is impeded by the development of hoop stresses as the material converges, reducing the layer's velocity. This allows time to reaccelerate the material behind the damaged region to catch up to the released layer. Magnetic drivers allow tailoring of the

amplitude and duration of the electrical pulse to produce the amount of damage and recollection desired in each experiment. In addition, the target is recoverable for post-experimental metallographic analysis, which provides data about the damage extent and distribution.

A. Experimental Load Configuration

The experiments studied the damage process in an inner cylindrical shell (target) impacted by an outer cylindrical shell (liner) launched by the magnetic pressure generated when an axial current is sent along its outer wall. Liner impact with the target sends a pressure wave through the target, which reflects off the inner wall creating tensile stresses (and perhaps damage) in the material. The amount of damage produced in the target depends on liner impact velocity and the thickness of the target. The driving current and location of the target control liner impact velocity. The thickness of the liner controls the shape of the pressure wave produced by the impact. Across the series, all targets were the same height, but varied in the radial direction to produce varying peak free surface velocities and, thus, damage conditions. A third cylindrical shell outside the liner (return conductor) provides a return path for the current.

Each load contained two aluminum targets, with different outer and inner radii but the same thickness, separated by a copper glide plane. Copper glide planes above and below the targets are used to hold the targets in plane until impact. Because of the greater strength of the copper compared to the aluminum, these glide planes reduce the motion of the liner in these areas, thus decreasing the dynamic inductance of the load. A schematic of the experimental configuration is shown in Fig. 1, with a cross-sectional view on the left and an axial view on the right. The dimensions are not to scale.

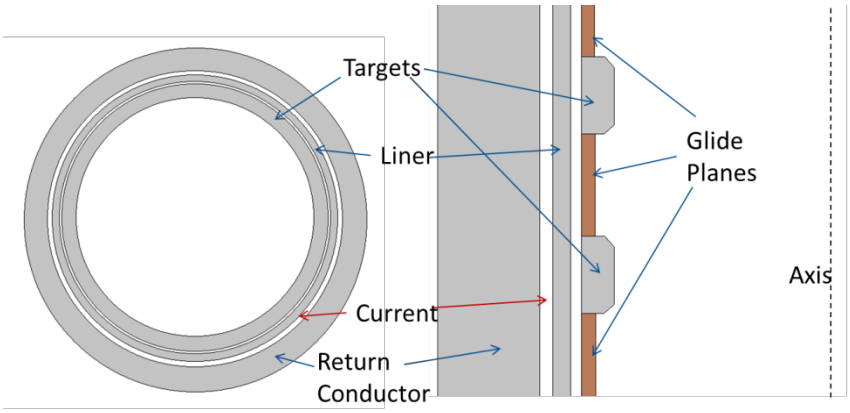

Fig. 1. Schematic of the experimental configuration (cross-section and axial).

B. Experimental Diagnostics

Six fiber-optic photon Doppler velocimetry (PDV) [1] probes were placed in a centrally located unit. For each target, the free (inner) surface velocity was measured in two places located 180 degrees apart. The remaining two probes were used to measure the free (inner) surface velocity of the incoming liner in two places. The liner measurement was accomplished by machining view ports through the middle glide plane. The current was measured with both inductive probes and Faraday rotation loops [2]. Measurements were taken in the generator, in the transmission line and in the load region. After the experiment, the load was recovered and metallographic analysis was performed on the targets.

III. Code Models

Accurate simulation of these experiments requires codes which contain all of the relevant physics. This includes models of material behavior, such as strength and damage, as well as models of electromagnetic effects, such as resistive diffusion and ohmic heating. Combining MHD capabilities with material modeling capabilities in a hydrocode allows for self-consistent end-to-end simulations of MHD-driven material property experiments.

A. Electromagnetic Models

A new capability for calculating resistive diffusion and ohmic heating using input current values has been added to a LANL Lagrangian hydrocode. Previously, simulations of these experiments used a magnetic boundary pressure condition as the driver. The resistive diffusion and ohmic heating are important as they allow the material in the liner to develop a more accurate temperature, density and velocity profile before impact with the target. Calculations show that the density in the outer third of the liner dropped by 1 – 2 percent before impact (see Fig. 2a), while the temperature increased from room temperature to approximately 600 K (see Fig. 2b). This reduces the support of the pressure wave, resulting in a wave that is no longer square, but rather drops off slightly on the back side. In turn, this reduces the amplitude of the velocity wave that is transmitted through the target and seen in the velocimetry data. The amplitude of the free-surface velocity is an important component in selection of parameter values for the strength and damage models.

(a) 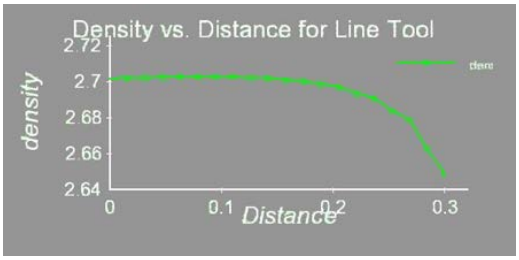

(b) 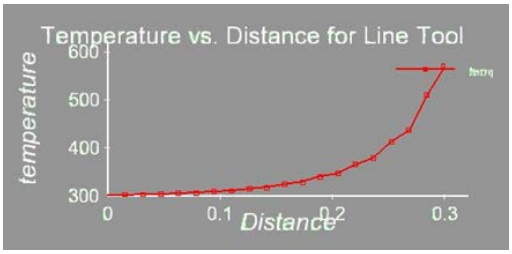

Fig. 2. Simulated (a) density and (b) temperature profile across liner at time of impact with target. Distance in cm, with 0 indicating the inner surface of the liner. Density in g/cm^3. Temperature in Kelvin.

B. Material Strength and Failure Models

The Preston-Tonks-Wallace (PTW) model [3] was used to model the material strength response to the applied load. The PTW model includes dependences on pressure, deviatoric strains, strain rates and temperatures. This model includes 11 parameter values to describe a material's behavior.

The Tepla model [4] was used to describe the material's tendency to damage and fail due to porosity growth and shear strains. The porosity growth rate is dependent on pressure, stresses and existing porosity. Porosity also affects the plastic flow surface and flow rate. The failure surface is described by a combination of porosity and strains. The model includes 9 parameter values to describe a material's behavior.

IV. Simulations

The largest issue for modeling the cylindrical damage experiments was the lack of knowledge about the particular aluminum alloy used in the experiments. From an analysis of the chemical composition, the alloy has been identified as Al-1060. This alloy is similar to the more commonly used Al-1100 in purity, but contains different impurities, namely, more manganese and less copper, iron, silicon and zinc. There were no available parameter values available for Al-1060 for any of the material models available in the code. Modeling attempts using the model parameters available for Al-1100 were not adequate.

A. Approach to Determining Parameter Values

The leading edge of the velocity at the free-surface of a target is dependent only on the material strength, as a tensile wave has not yet been produced. The elastic foot and the amplitude of the velocity pulse were used to adjust the PTW strength parameters by searching through a range of values centered at the known parameter values for other aluminum alloys. Basically, Al-1060 has a significantly smaller yield stress than Al-1100 at all temperatures.

A similar approach was used for determining the Tepla failure model parameter values. Using available parameter values for other aluminum alloys provided a starting point. Then half of the cylindrical damage experiments were used in a parametric search to optimize the Tepla parameter values for this material. The chosen values were then applied in simulations of the remaining targets. A simple porosity removal model is used, where porosity removal occurs at a rate equal to, but opposite sign of, porosity growth.

B. Results

The first consideration of simulation results is whether the motion of the liner is adequately captured. Accurate liner motion is needed to produce the correct pressure pulse in the target. The simulated results of the liner motion for the four experiments are shown in comparison to the velocimetry data in Fig. 3. The calculated results are shown in red, while the two data measurements are shown in blue and green. In the simulations, the liner impacts the target at the point where the red velocity trace drops rapidly. In the data, the liner is being viewed through a port, thus its velocity continues to increase and then rings as waves from the edges of the viewport arrive at the point of measurement. Time is in microseconds and velocity in meters per second. The liner simulations are quite reasonable.

(a)

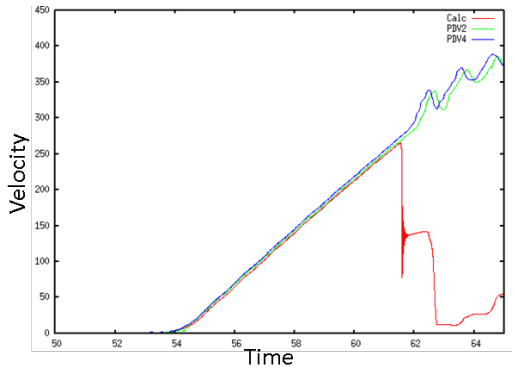

(b)

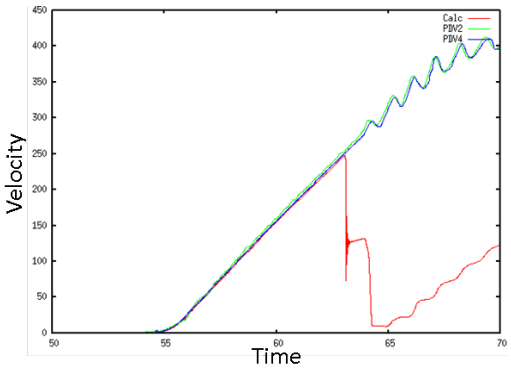

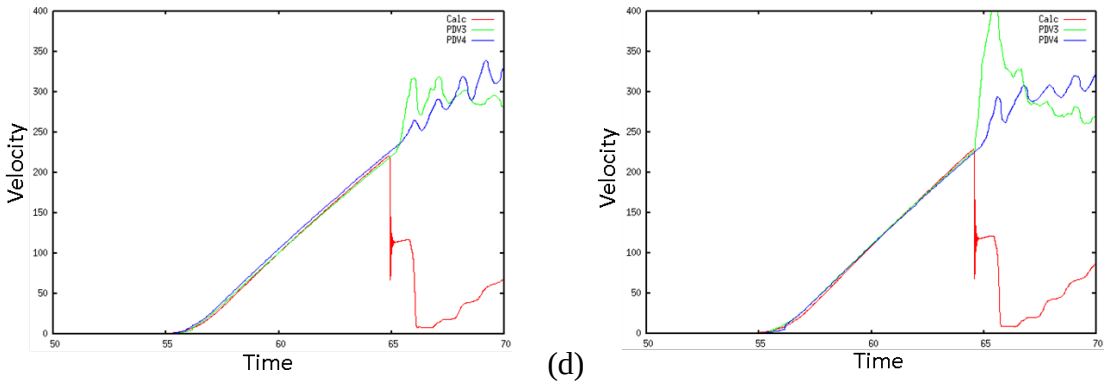

(c) (d)

Fig. 3. Simulated liner motion (red) vs. data (blue, green) for Experiments 6 – 9 (a – d).

Next, the simulation results for the targets are considered. There are two targets in each experimental load and there are four experiments considered, for a total of eight targets. The targets in Experiments 6 and 7 were used to develop the Tepla parameter values. Those values were then applied to Experiments 8 and 9. The simulated results are shown in Fig. 4 - 11, with the calculated results in red and the experimental data in blue and green. On the left is the entire trace of the velocimetry for each target; on the right, is a magnified view of the initial part of the velocimetry trace. Each trace is labeled by the experiment number and target outer radius. Velocity is in units of meters per second. Time is in microseconds measured from generator firing. The target simulations are quite acceptable.

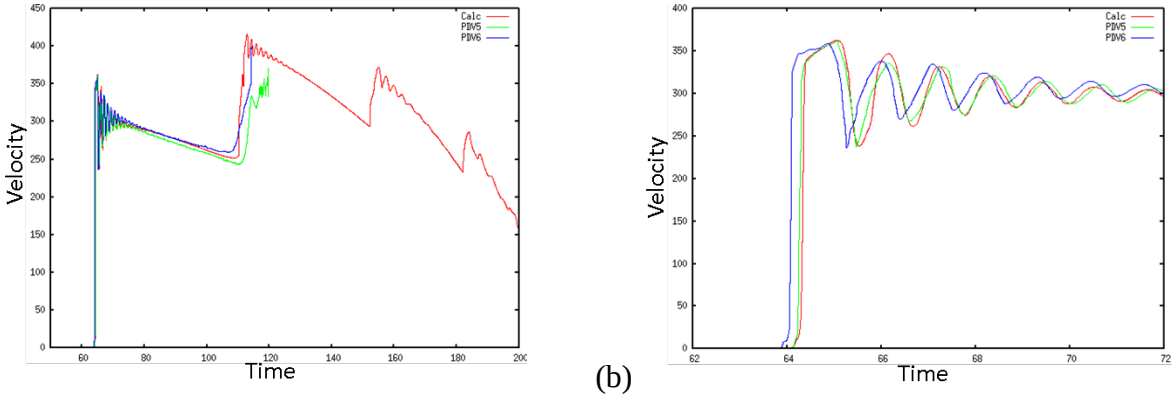

(a) (b)

Fig. 4. Experiment 6, 55.5 mm target. Simulated (red) vs. data (blue, green).

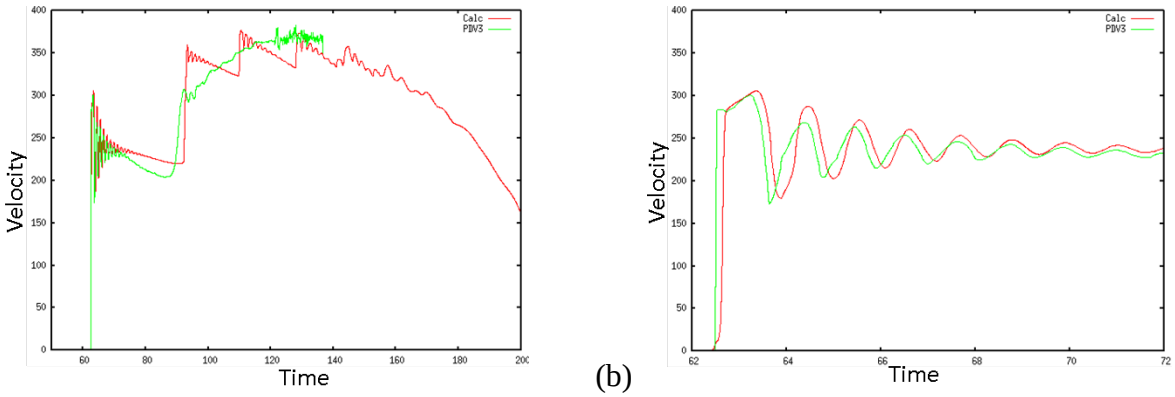

(a) (b)

Fig. 5. Experiment 6, 56 mm target. Simulated (red) vs. data (green).

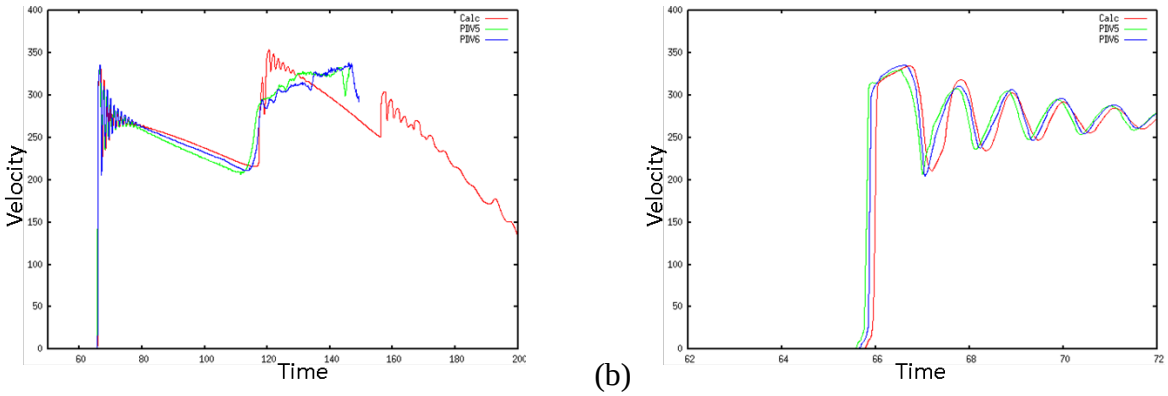

(a) (b)

Fig. 6. Experiment 7, 55.5 mm target. Simulated (red) vs. data (blue, green).

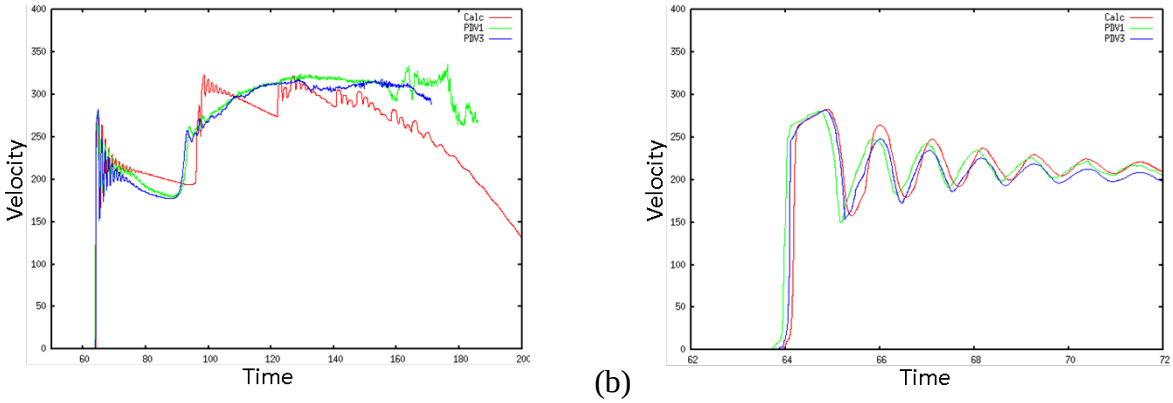

(a) (b)

Fig. 7. Experiment 7, 56 mm target. Simulated (red) vs. data (blue, green).

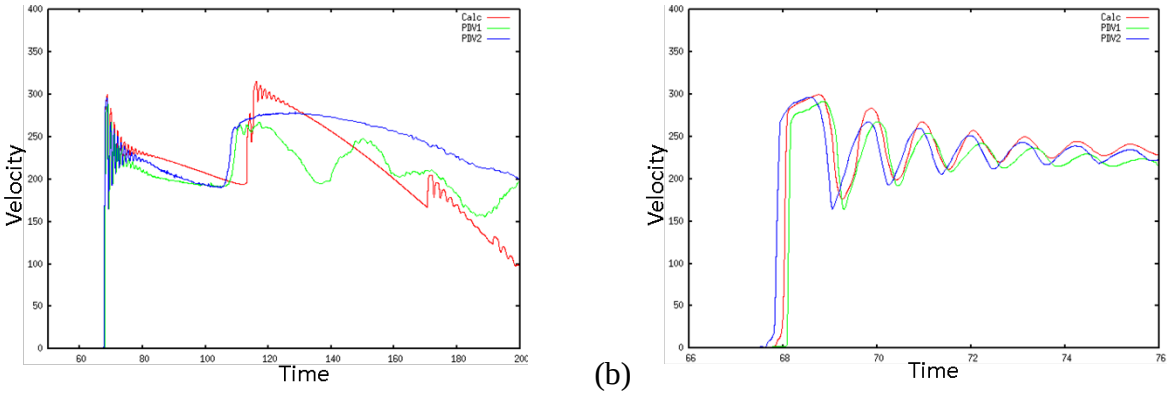

(a) (b)

Fig. 8. Experiment 8, 55.5 mm target. Simulated (red) vs. data (blue, green).

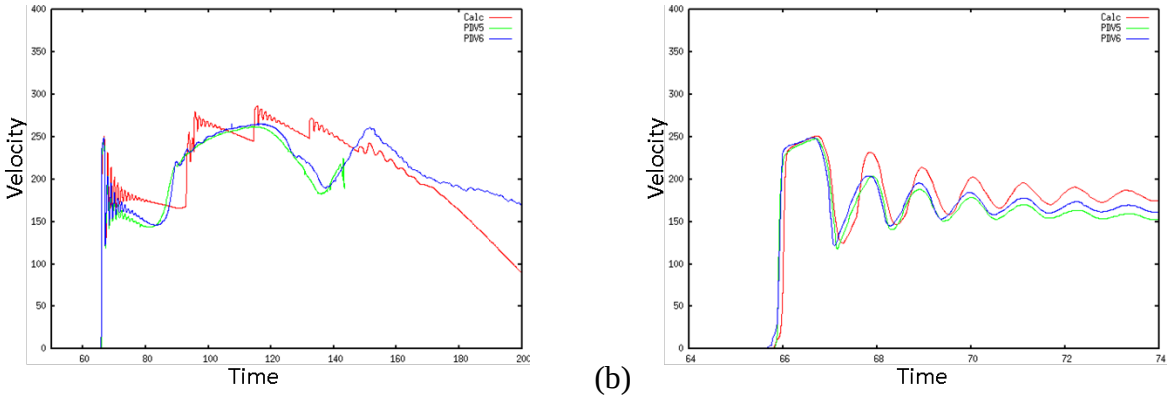

(a) (b)

Fig. 9. Experiment 8, 56 mm target. Simulated (red) vs. data (blue, green).

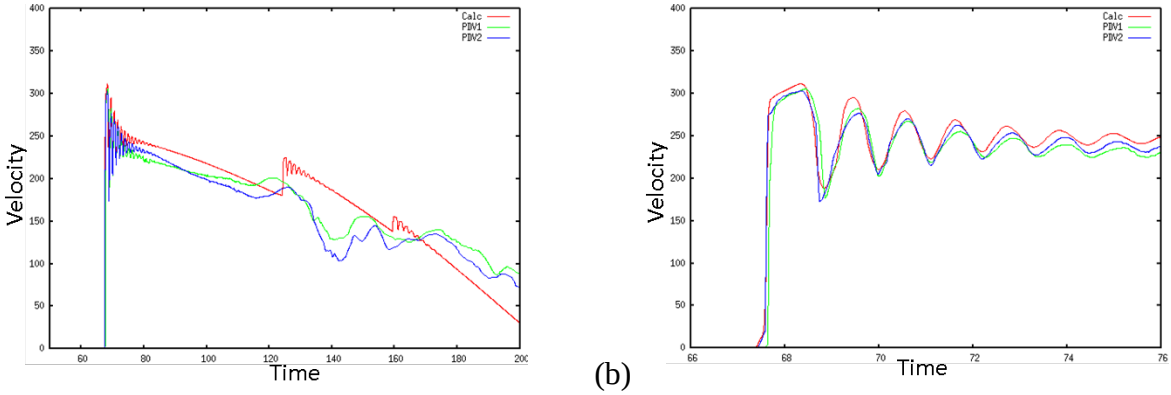

(a) (b)

Fig. 10. Experiment 9, 55.5 mm target. Simulated (red) vs. data (blue, green).

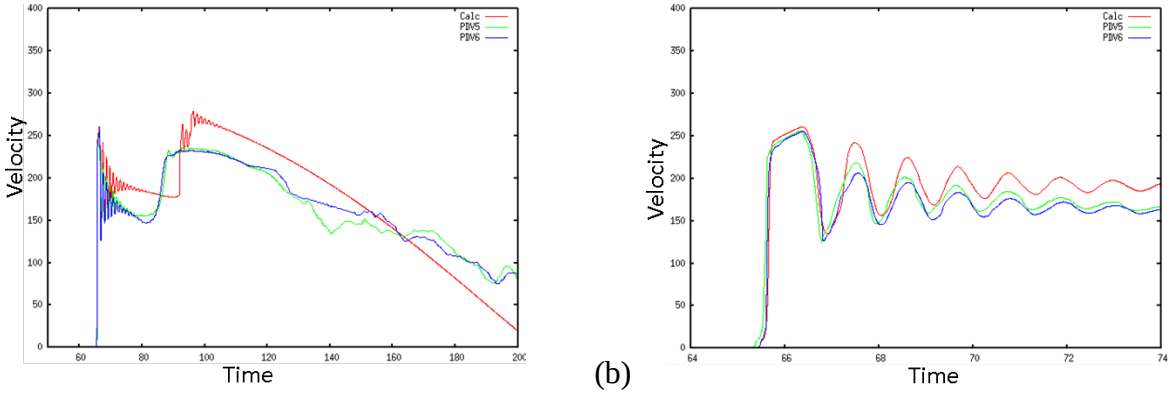

(a) (b)

Fig. 11. Experiment 9, 56 mm target. Simulated (red) vs. data (blue, green).

V. Conclusions

This series of joint experiments between LANL and VNIIEF has produced a proven technique for obtaining failure and recollection data using a magnetically-driven cylindrical load. A new capability for calculating resistive diffusion and ohmic heating using input current values has been added to a LANL Lagrangian hydrocode, allowing a more accurate calculation of the liner behavior prior to impact with the target, which in turn allows a more accurate calculation of the target response. Using the well-characterized data from these experiments, strength and failure model parameter values have been established for aluminum-1060. The combination of magneto-

hydrodynamics (MHD) and material modeling capabilities in a Lagrangian hydrocode allows for self-consistent end-to-end simulations of MHD-driven material property experiments.

Acknowledgments
The author gratefully acknowledges the efforts of the LANL and VNIIEF experimental teams.

References
[1] Strand, O. T., et al., “Compact system for highspeed velocimetry using heterodyne techniques,” Rev. Sci. Instr. 77 (2006) 083108
[2] Veeser, L. and Day. G., “Fiber optic, Faraday rotation current sensor,” Proceedings of the Fourth International Conference on Megagauss Magnetic Field Generation and Related Topics (1987) 323 -30.
[3] Preston, D. L., Tonks, D. L., Wallace, D. C., “Model of plastic deformation for extreme loading conditions,” J. Appl. Phys. 93 (2003) 211-220
[4] Addessio, F. N. and Johnson, J. N., “Rate-dependent ductile failure model,” J. Appl. Phys. 74-3 (1993) 1640-1648

---

* This work was performed under the auspices of the U.S. Department of Energy by Los Alamos National Laboratory under Contract DE-AC52-06NA25396.